Ab initio study of the structural, electronic, and phononic properties of $Nb_{1-x}Mo_x$ using the self-consistent virtual-crystal approximation

O. De la Peña-Seaman,[1,2] R. de Coss,[1] R. Heid,[2] and K.-P. Bohnen[2]
[1]*Departamento de Física Aplicada, Centro de Investigación y de Estudios Avanzados del IPN, Apartado Postal 73, Cordemex 97310 Mérida, Yucatán, México*
[2]*Forschungszentrum Karlsruhe, Institut für Festkörperphysik, P.O. Box 3640, D-76021 Karlsruhe, Germany*
(Received 26 June 2007; revised manuscript received 9 October 2007; published 15 November 2007)

We have studied the structural, electronic, and lattice dynamics properties of $Nb_{1-x}Mo_x$ alloy within the framework of density functional theory using the self-consistent virtual-crystal approximation (VCA). The structural properties, electronic band structure, and selected high-symmetry phonon frequencies have been calculated for the entire range of Mo concentrations comparing two implementations, an all-electron and a pseudopotential method. We found very good agreement between both methodologies for all calculated properties, independent of the approximation used for the exchange-correlation functional. We identified an electronic topological transition for this alloy at around 30% of Mo content. For all properties considered, we found good agreement with experimental results, indicating the applicability of the VCA for this alloy.

DOI: 10.1103/PhysRevB.76.174205 PACS number(s): 71.20.Be, 71.15.Mb, 61.82.Bg, 63.20.Dj

I. INTRODUCTION

The $Nb_{1-x}Mo_x$ alloy forms a solid solution with a body-centered cubic (bcc) structure for the entire range of Mo concentrations ($0.0 \leqslant x \leqslant 1.0$).[1,2] The constituent elements, Nb and Mo, belong to the 4*d* transition metals of the Periodic Table with 5 and 6 valence electrons, respectively. Therefore, by changing the Mo content in the system, we obtain a continuous variation of the number of electrons per atom (N_e). An interesting characteristic of this system is the nonmonotonic behavior of the superconducting critical temperature (T_c) as a function of x. While Nb possesses the highest T_c among elemental metals (9.25 K), T_c falls below 0.5 K at $x \approx 0.4$, recovers again at higher Mo content, and reaches a T_c of 0.92 K for pure Mo.[1,2]

The nonmonotonic behavior of T_c for the Nb-Mo alloy as a function of the Mo content has motivated many experimental and theoretical studies. Indeed, there are a lot of studies on the structural,[2–6] electronic,[7–14] vibrational,[15–23] and superconducting properties[1,23–26] of this alloy. It is interesting to note that the evolution of these properties as a function of Mo content is sometimes nonmonotonic. The origin of these features are not yet completely understood despite all the above mentioned efforts. For example, experimental studies of the elastic properties at low temperatures show anomalies in the C' and C_{44} elastic constants around a Mo content of $x \approx 0.4$.[4,6,27–29] This behavior was associated with an electronic topological transition of the Fermi surface as a consequence of increasing N_e. However, early tight-binding calculations of the electronic structure and elastic properties for this alloy using the rigid band approximation did not reproduce the anomalies observed experimentally.[4,6,27–29]

Another interesting behavior comes from the vibrational properties, where the evolution of the dispersion curves with increasing Mo content shows that the phonon anomalies are strongly dependent on the value of N_e.[15–17] For example, on the one hand, a Kohn anomaly is present in the longitudinal branch $[00\zeta]$ in Nb, but not in Mo. On the other hand, in Mo, a depression is found near the symmetry point *H* for the longitudinal and transversal branches.[15–17] The evolution of this anomaly in the $Nb_{1-x}Mo_x$ alloy was studied using coherent one-phonon scattering of thermal neutrons and it was found that at $x \approx 0.4$, the anomaly starts to disappear,[17] but for higher Mo concentrations ($\geqslant 0.9$), a depression at the *H* point appears suddenly. Another example of this type of changes due to the variation of N_e occurs in the transversal-mode frequencies at the *N* point, where the frequencies of T_1 and T_2 in Nb are 16.13 and 20.88 meV, respectively, while for Mo this ordering is reversed with the T_2 frequency at 18.78 meV and the T_1 at 23.57 meV.[17] From the theoretical point of view, the evolution of the electronic and elastic properties of the $Nb_{1-x}Mo_x$ alloy as a function of x has been studied using quasirandom structures,[5] the coherent potential approximation,[10–12] and the Korringa-Kohn-Rostoker coherent potential approximation.[13,14] However, these studies have been limited to only a few Mo concentrations because these calculations are computationally very demanding, especially if one is interested in very low (close to Nb) or high concentrations (close to Mo). These studies[10–12,14] found an electronic topological transition (ETT) from a holelike band to an electronlike band at the Γ point of the electronic band structure between $x=0.25$ and $x=0.50$, but because a large disorder-induced smearing of the bands was already obtained for the $x=0.25$ case, it was difficult to accurately identify the critical Mo concentration (x_c) of the ETT in this alloy. A smaller range $x_c=0.3-0.4$ was given by Bruno *et al.*,[13] who analyzed the ETT within the rigid-band approximation using their calculated band structure for $x=0.50$ as a starting point.

In this paper, we present a study of the structural, electronic, and vibrational properties of the $Nb_{1-x}Mo_x$ alloy for $0.0 \leqslant x \leqslant 1.0$, within the framework of density functional theory[30] using the self-consistent virtual-crystal approximation (VCA).[31,32] We performed the calculations using the full-potential linearized augmented plane-wave method (LAPW)[33–35] as implemented in the WIEN2K code[36] for which the VCA has already been tested on other systems.[31,32] In addition, we investigated the same properties using an implementation of the VCA within the mixed-basis pseudopoten-

tial (MBPP) method.[37] The current MBPP code incorporates an implementation of the very efficient linear response approach to lattice dynamical properties, which is currently not available in the WIEN2K code. The present work serves partly to test and validate with high accuracy the VCA implementation within MBPP with the aim to use it for a more complete analysis of phonon spectra and electron-phonon interactions in future work. For this purpose, we have selected a very simple, yet widely studied system: the Nb-Mo alloy. The evolution of structural parameters is presented, and the behavior of the electronic band structure as a function of Mo content is analyzed in order to determine the critical concentration of the electronic topological transition. For high-symmetry points at the Brillouin-zone boundary (H,N), we compare in detail phonon frequencies obtained with the frozen-phonon approximation (FPA) using the LAPW method[33–35] and with the linear response theory (LRT)[38–41] as implemented in the MBPP code. Since it is well known that the degree of agreement with experimental results may depend on the treatment of the exchange correlation, we have used two types of exchange-correlation (xc) functionals, the local density approximation (LDA) and the generalized gradient approximation (GGA) for both methodologies.

II. COMPUTATIONAL DETAILS

For the all-electron calculations, the Kohn-Sham total energies were calculated self-consistently using the full-potential LAPW[33–35] method as implemented in the WIEN2K code.[36] The core states were treated fully relativistically, and the semicore and valence states were computed in a scalar-relativistic approximation.[42] The exchange-correlation potential was evaluated within the LDA using the Perdew-Wang form[43] and the GGA using the functional proposed by Perdew, Burke, and Ernzerhof[44–46] (PBE). We chose muffin-tin radii (R_{MT}) of 2.25 a.u. for Nb and Mo, and a plane-wave cutoff $R_{MT}\times K_{MAX}=9.0$. Inside the atomic spheres, the potential and charge densities were expanded in crystal harmonics up to $l=10$. Convergence was assumed when the energy difference between the input and output steps was less than 1×10^{-6} Ry. Special attention was paid to the convergence of results with respect to the number of k points. We used a grid of $23\times23\times23$ for the structural optimization and $32\times32\times32$ for the frozen-phonon calculations. The Brillouin-zone integration was carried out with the Gaussian smearing method with a smearing factor of 0.2 eV. The vibrational properties obtained with the LAPW code were calculated using the FPA,[19,21,22] which involves the calculation of the total energy of the crystal as a function of atom displacements for a particular eigenmode. The phonon modes studied correspond to the wave vector at the H (threefold degenerated) and N high-symmetry points. The energy-versus-displacement surface was fitted by a sixth-order polynomial with only even terms, as required by the symmetry of the displacement patterns. The harmonic phonon frequency was then extracted from the second-order coefficient of the fitted polynomial.

The pseudopotential calculations were performed with the MBPP.[37] In this calculation, we have considered $4s$ and $4p$ semicore states as valence electrons which substantially improved the description of the different calculated properties in this alloy. The fairly deep potentials for Nb/Mo are efficiently treated by the mixed-basis scheme, which uses a combination of local functions and plane waves for the representation of the valence states. We used s-, p-, and d-type functions at the Nb/Mo sites, supplemented by plane waves up to a kinetic energy of 36 Ry. Phonon properties are calculated via density functional perturbation theory[30,47] as implemented in the MBPP code.[38,40] The studies were carried out with two different approximations for the exchange-correlation functional, the LDA using the Hedin-Lundqvist form[48] and the GGA using the PBE functional.[44–46] The Brillouin-zone integration has been performed using Monkhorst-Pack special k-point sets with a Gaussian smearing of 0.2 eV. For the calculation of the ground state properties (structural optimization and electronic properties), a $20\times20\times20$ k-point mesh was used. For the phonon calculations, we used a much denser $32\times32\times32$ k-point mesh.

The $Nb_{1-x}Mo_x$ alloy was modeled in the self-consistent VCA.[31,32,49–51] In the case of the all-electron method, the Nb $(Z=41)$ sites were substituted by pseudoatoms which have a fractional electronic charge $(Z=41+x)$ depending on the Mo concentration (x). The valence charge was modified by the same amount in order to maintain the neutrality of the pseudoatom. This approximation is justified since Mo has only one electron more than Nb. The potential for the VCA system is determined self-consistently for each value of x without shape approximation.[36] The self-consistent VCA within the LAPW framework has already been applied successfully to model C, Be, and Al substitutions in MgB_2 (Refs. 31 and 32) and electron and hole doping in high-temperature superconducting compounds.[50,51] In the same spirit, the VCA is implemented within the pseudopotential method by generating new pseudopotentials with a fractional nuclear charge $(Z=41+x)$ for each x and by adjusting the valence charge accordingly. The equilibrium lattice parameters were determined by total-energy calculations for each value of Mo concentration ($x=0.0$, 0.1, 0.2, 0.3, 0.4, 0.5, 0.6, 0.7, 0.8, 0.9, and 1.0). The structural optimization was performed with both methods, all-electron (LAPW) and pseudopotential (MBPP), and for each method with both xc functionals, LDA and GGA.

III. RESULTS AND DISCUSSION

In Fig. 1, we show the evolution of the lattice parameter (a_0) and the bulk modulus (B_0) as a function of Mo content. The very good agreement between the two methods of calculation for the same xc functional (LDA or GGA) indicates that the implementation of the VCA in the pseudopotential code describes very well the structural parameters of the Nb-Mo alloy. In fact, both methods with both functionals follow the trend of the experimental data. The GGA results are closer to the experimental data than LDA, which is consistent with the tendency found in the literature that GGA improves the calculation of the lattice parameters in comparison with LDA.[52–57] The largest difference between our GGA calculations and the experimental data for a_0 is only

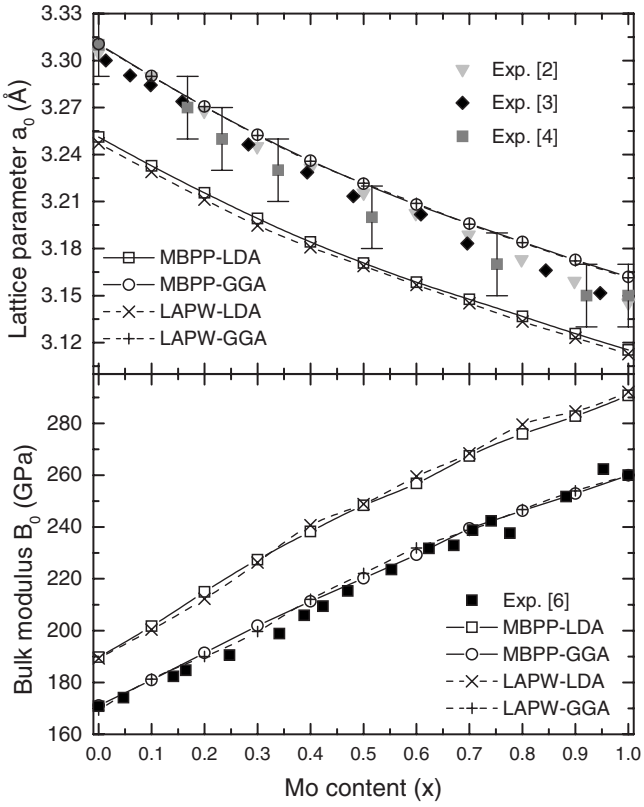

FIG. 1. Lattice parameter (a_0) and bulk modulus (B_0) for the $Nb_{1-x}Mo_x$ alloy as a function of x.

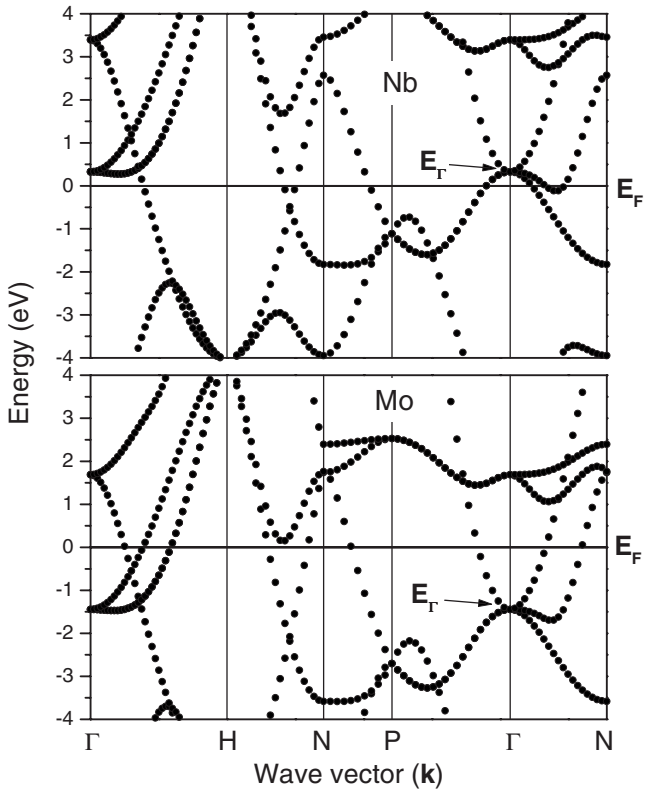

FIG. 2. Electronic band structure for Nb and Mo in the bcc structure.

0.5%, which is obtained for pure Mo with the MBPP-GGA value of 3.1619 Å and the experimental value of 3.1454 Å.[2]

In order to evaluate the effects of increasing the Mo content on the electronic properties of the alloy, we analyzed the evolution of the electronic band structure. In Fig. 2, we show the band structures for the boundary cases for this alloy, Nb(x=0) and Mo(x=1), which were calculated using MBPP-GGA optimized lattice parameters.

From the band structure, it can be seen that a threefold degenerated state exists at the Γ point (E_Γ) (Ref. 61) close to the Fermi level, which lies at 0.3 eV in Nb and at −1.5 eV in Mo. Thus, in Nb (x=0), the band centered at Γ is unfilled and crosses the Fermi level with hole character, but as the Mo content is increased, this band starts to fill up until a critical concentration (x_c) where this band is completely filled. For $x > x_c$, other bands are rising in that region but with electron character. This indicates that an ETT occurs at x_c since the Fermi surface corresponding to the holelike band disappears and a Fermi surface with electron character emerges. In order to find the critical concentration x_c, we trace the evolution of the energy bands at the Γ point. In Fig. 3, these values are shown as a function of x calculated with both methods and both functionals, obtaining a very good agreement between both methods, MBPP and LAPW. Also, we find that GGA gives slightly larger values for x_c than LDA (x_c is 0.28 and 0.32 for LDA and GGA, respectively). Note that this result represents an accurate determination (under the restrictions and limits of VCA) for $x_c \approx 0.3$ of the ETT, which has been conjectured from the observed anomalies in the elastic properties of this system.[6]

As mentioned before, we have calculated the phonon frequencies of the $Nb_{1-x}Mo_x$ alloy at the H and N high-symmetry points by means of the FPA using the all-electron code (LAPW) and with the LRT implemented in the pseudopotential code (MBPP), in order to compare the results obtained with the two methods using both LDA and GGA functionals to experimental data. The results for the phonon frequencies are presented in Figs. 4 and 5, where the label FPA indicates frequencies obtained with the LAPW code and LRT indicates the ones obtained with MBPP. For compari-

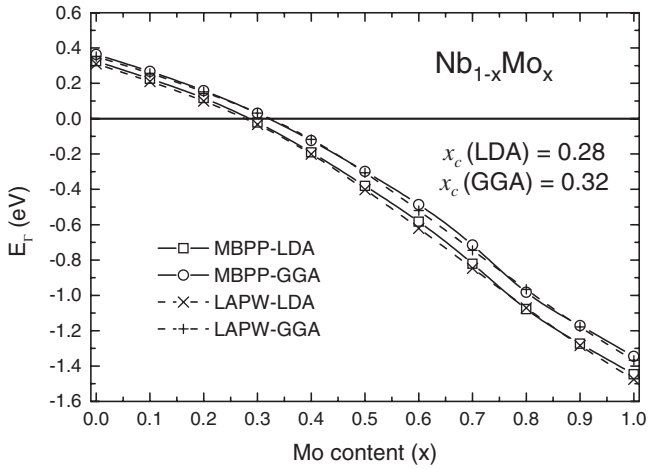

FIG. 3. Evolution of E_Γ as a function of x for the $Nb_{1-x}Mo_x$ alloy.

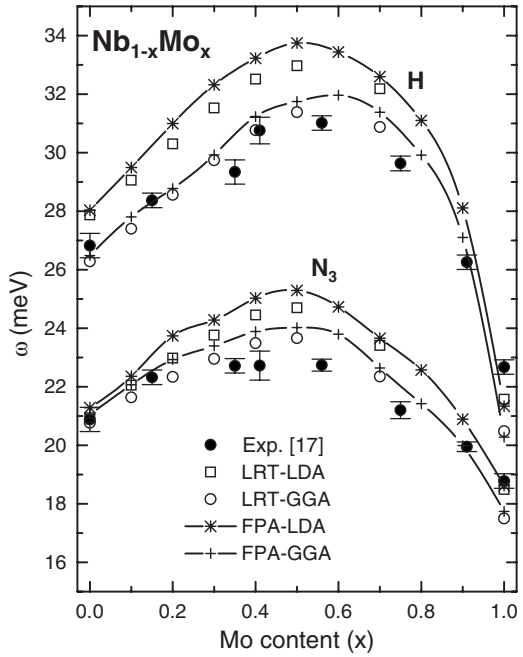

FIG. 4. Frequency of the H and N_3 phonon modes for the $Nb_{1-x}Mo_x$ alloy as a function of x. LRT calculations correspond to the MBPP code and FPA calculations correspond to the LAPW code.

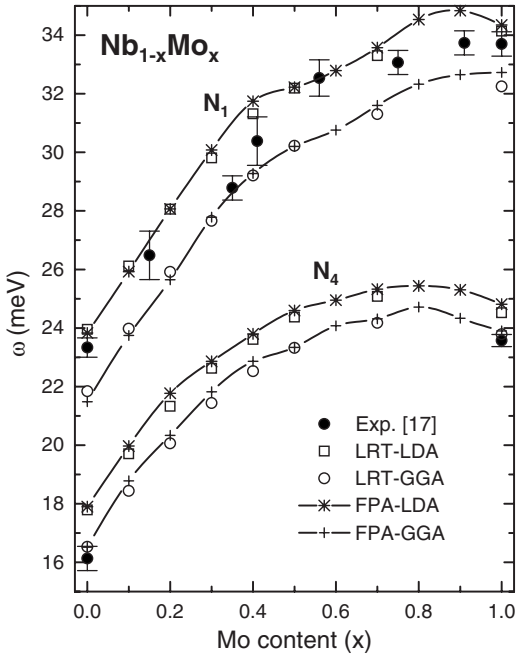

FIG. 5. Frequency of the N_1 and N_4 phonon mode for the $Nb_{1-x}Mo_x$ alloy as a function of x. LRT calculations correspond to the MBPP code and FPA calculations correspond to the LAPW code.

son, experimental frequencies from Powell *et al.*[17] are included. These data were taken at room temperature, but it has been found that the frequencies of the H- and N-point phonons practically remain unchanged down to low temperatures.[58,59] We see that the frequencies agree very well between the two methodologies (FPA and LRT). Furthermore, the trends of the experimental data are reproduced with both functionals, LDA and GGA. The nonmonotonic dependence of the frequencies on x is a very remarkable result in view of the fact that the VCA works as a linear interpolation of the electronic charge at the beginning of the calculation. However, due to the self-consistent treatment, the charge density is redistributed, thus leading to a better description of the alloy than, for example, the rigid-band approximation, which only considers the shifting of the Fermi level as the principal effect of alloying.

From Fig. 4, we can see that for both modes H and N_3, the frequency shows a monotonic increase until $x \approx 0.4-0.5$ where it reaches a maximum, and then starts to decrease for larger x. We note that for the frequency of the H mode in Mo, a slight deviation is observed from the experimental value ($\omega_{FPA\text{-}LDA}=21.34$ meV, $\omega_{FPA\text{-}GGA}=20.28$ meV, $\omega_{expt}=22.68\pm0.25$ meV) despite the fact that anharmonic terms have been taken into account. Extensive tests showed that the frequency of the H-point phonon of Mo is quite sensitive to various numerical parameters, such as k-point sampling, because of the presence of an anomaly at the H point. Interestingly, both methods with both functionals give very similar frequencies (a difference of less than 0.4 meV) for the N_3 mode in Nb which is also anomalous. For the N_1 mode (see Fig. 5), we found a quasilinear behavior of the frequency as a function of x for $x \leqslant 0.4$, with a large slope. In contrast to the other modes studied, the N_1 mode does not show a maximum for intermediate concentrations. Finally, for the N_4 mode, we found good agreement with the experimental frequency at the boundary values of x (Nb and Mo) in the case of GGA. Further experimental data are not available for this specific mode.

From the methodological point of view, we found that the range of differences between the calculated frequencies with GGA and LDA is quite broad, but it depends on the mode. For instance, for the H and N_1 modes ($\Delta\omega_{LDA\text{-}GGA} \approx 1.24-2.48$ meV), the differences are larger than those for the N_3 and N_4 modes ($\Delta\omega_{LDA\text{-}GGA} \approx 0.41-1.65$ meV). This indicates that the H and N_1 modes are more sensitive to the xc functional and, in general, to the details of the description of the electronic density of the system. We find that in both methods, GGA gives lower frequencies than LDA and that GGA is in better agreement with the experimental results, with the exception of the N_1 mode where both LDA and GGA show the same level of agreement. However, more calculations for the phonon dispersion curves are needed in order to establish which xc functional better describes the phonon properties of the Nb-Mo alloy system. Finally, we note that the differences of the frequencies between calculations and experiments could be larger if the numerical parameters are not properly taken into account. In particular, for the FPA, the fitting procedure of the effective potential to the total-energy calculations is rather critical in order to get reliable results. For example, for the H and N phonons, it was necessary to use at least a sixth-order polynomial.

IV. CONCLUSIONS

We have performed a first-principles study of the complete alloy series $Nb_{1-x}Mo_x$ as a function of x of the struc-

tural parameters, the electronic structure, and the phononic frequencies at the *H* and *N* points, using the virtual-crystal approximation. In general, we found very good agreement with experimental trends for all properties investigated. This also includes the nonmonotonic behavior of the frequencies at the *H* and *N* points, indicating that VCA works well describing this alloy system. The self-consistent VCA implemented in the pseudopotential mixed-basis code works very well for the Nb-Mo alloy, as deduced by comparison to the all-electron calculations of the structural, electronic, and vibrational properties. We accurately determined $x_c \approx 0.3$ for the ETT present at the Γ point, where the Fermi surface corresponding to the holelike band disappears and a Fermi surface with electron character emerges. This ETT has been related with the observed anomalies in the elastic properties of this alloy. The analysis performed using two different xc functionals shows that with respect to structural properties, GGA agrees better with experimental data than LDA. We find that the GGA calculations for the phonon frequencies of the *H* and *N* modes in $Nb_{1-x}Mo_x$ are in better agreement with experimental data than the corresponding LDA calculations. However, more calculations for the phonon dispersion curves are needed, in order to establish a more general conclusion about the quality of the xc functional describing the phonon properties for this alloy system.

The successful VCA implementation in the MBPP code, as demonstrated above, opens the way for investigations of the complete phonon dispersion curves and electron-phonon coupling properties for this alloy system, which will be the topic of a forthcoming paper.[60]

ACKNOWLEDGMENTS

This research was supported by the Consejo Nacional de Ciencia y Tecnología (CONACYT, México) under Grant No. 43830-F and the Forschungszentrum Karlsruhe, Germany. One of the authors (O.P.-S.) gratefully acknowledges a student award from CONACYT-México and the support from the Forschungszentrum Karlsruhe.

[1] J. Hulm and R. Blaugher, Phys. Rev. **123**, 1569 (1961).
[2] H. J. Goldschmidt and J. A. Brand, J. Less-Common Met. **3**, 44 (1961).
[3] J. A. Catterall and S. M. Barker, Plansee Proceedings (Springer, Vienna, 1964), p. 577.
[4] W. C. Hubbell and F. R. Brotzen, J. Appl. Phys. **43**, 3306 (1972).
[5] C. Jiang, C. Wolverton, J. Sofo, L. Q. Chen, and Z. K. Liu, Phys. Rev. B **69**, 214202 (2004).
[6] P. Bujard, R. Sanjines, E. Walker, J. Ashkenazi, and M. Peter, J. Phys. F: Met. Phys. **11**, 775 (1981).
[7] W. M. Lomer, Proc. Phys. Soc. London **80**, 489 (1962).
[8] L. F. Mattheiss, Phys. Rev. **139**, A1893 (1965).
[9] T. L. Loucks, Phys. Rev. **139**, A1181 (1965).
[10] E. Colavita, A. Franciosi, R. Rosei, F. Sacchetti, E. S. Giuliano, R. Ruggeri, and D. W. Lynch, Phys. Rev. B **20**, 4864 (1979).
[11] E. Donato, B. Ginatempo, E. Giuliano, R. Rugger, and A. Stancanell, J. Phys. F: Met. Phys. **12**, 2309 (1982).
[12] C. R. Bull, J. H. Kaiser, A. Alam, N. Shiotani, and R. N. West, Phys. Rev. B **29**, 6378 (1984).
[13] E. Bruno, B. Giantempo, E. S. Giuliano, A. V. Ruban, and Y. K. Vekilov, Phys. Rep. **249**, 353 (1994).
[14] S. S. Rajput, R. Prasad, R. M. Singru, S. Kaprzyk, and A. Bansil, J. Phys.: Condens. Matter **8**, 2929 (1996).
[15] Y. Nakagawa and A. D. B. Woods, Phys. Rev. Lett. **11**, 271 (1963).
[16] A. D. B. Woods and B. M. Powell, Phys. Rev. Lett. **15**, 778 (1965).
[17] B. M. Powell, P. Martel, and A. D. B. Woods, Phys. Rev. **171**, 727 (1968).
[18] C. M. Varma and W. Weber, Phys. Rev. B **19**, 6142 (1979).
[19] K. M. Ho, C. L. Fu, B. N. Harmon, W. Weber, and D. R. Hamann, Phys. Rev. Lett. **49**, 673 (1982).
[20] J. Zarestky, C. Stassis, B. N. Harmon, K. M. Ho, and C. L. Fu, Phys. Rev. B **28**, 697 (1983).
[21] Y. Chen, C. L. Fu, K. M. Ho, and B. N. Harmon, Phys. Rev. B **31**, 6775 (1985).
[22] D. Singh and H. Krakauer, Phys. Rev. B **43**, 1441 (1991).
[23] S. Y. Savrasov and D. Y. Savrasov, Phys. Rev. B **54**, 16487 (1996).
[24] J. Bostock, V. Diadiuk, W. N. Cheung, K. H. Lo, R. M. Rose, and M. L. MacVicar, Phys. Rev. Lett. **36**, 603 (1976).
[25] R. Bauer, A. Schmid, P. Pavone, and D. Strauch, Phys. Rev. B **57**, 11276 (1998).
[26] C. M. Perlov and C. Y. Fong, Phys. Rev. B **29**, 1243 (1984).
[27] R. L. Cappelletti, N. Wakabayashi, W. A. Kamitakahara, J. G. Traylor, and A. J. Bevolo, Phys. Rev. B **25**, 6096 (1982).
[28] P. C. Camargo, F. R. Brotzen, and S. Steinemann, J. Phys. F: Met. Phys. **17**, 1065 (1987).
[29] J. Ashkenazi, M. Dacorogna, M. Peter, Y. Talmor, E. Walker, and S. Steinemann, Phys. Rev. B **18**, 4120 (1978).
[30] J. W. Kohn and L. J. Sham, Phys. Rev. **140**, A1133 (1965).
[31] M. J. Mehl, D. A. Papaconstantopoulos, and D. J. Singh, Phys. Rev. B **64**, 140509(R) (2001).
[32] O. de la Peña, A. Aguayo, and R. de Coss, Phys. Rev. B **66**, 012511 (2002).
[33] O. K. Andersen, Phys. Rev. B **12**, 3060 (1975).
[34] D. D. Koelling and G. O. Arbman, J. Phys. F: Met. Phys. **5**, 2041 (1975).
[35] D. J. Singh, *Plane Waves, Pseudopotentials and the LAPW Method* (Kluwer Academic, Boston, 1994).
[36] P. Blaha, K. Schwarz, G. K. H. Madsen, D. Kvasnicka, and J. Luitz, *WIEN2k, An Augmented Plane Wave+Local Orbitals Program for Calculating Crystal Properties* (Tech. Universität Wien, Vienna, 2001).
[37] B. Meyer, C. Elsässer, and M. Fähnle, FORTRAN90, program for mixed-basis pseudopotential calculations for crystals, Max-Planck-Institut für Metallforschung, Stuttgart.
[38] S. Baroni, P. Giannozzi, and A. Testa, Phys. Rev. Lett. **58**, 1861 (1987).
[39] P. Giannozzi, S. de Gironcoli, P. Pavone, and S. Baroni, Phys.

Rev. B **43**, 7231 (1991).
[40] R. Heid and K. P. Bohnen, Phys. Rev. B **60**, R3709 (1999).
[41] R. Heid, K. P. Bohnen, and K. M. Ho, Phys. Rev. B **57**, 7407 (1998).
[42] D. D. Koelling and B. N. Harmon, J. Phys. C **10**, 3107 (1977).
[43] J. P. Perdew and Y. Wang, Phys. Rev. B **45**, 13244 (1992).
[44] V. Ozolins and M. Korling, Phys. Rev. B **48**, 18304 (1993).
[45] K. Kokko and M. P. Das, J. Phys.: Condens. Matter **10**, 1285 (1998).
[46] J. P. Perdew, K. Burke, and M. Ernzerhof, Phys. Rev. Lett. **77**, 3865 (1996).
[47] S. G. Louie, K. M. Ho, and M. L. Cohen, Phys. Rev. B **19**, 1774 (1979).
[48] L. Hedin and B. I. Lundqvist, J. Phys. C **4**, 2074 (1971).
[49] D. A. Papaconstantopoulos, E. N. Economou, B. M. Klein, and L. L. Boyer, Phys. Rev. B **20**, 177 (1979).
[50] C. Ambrosch-Draxl, P. Süle, H. Auer, and E. Y. Sherman, Phys. Rev. B **67**, 100505(R) (2003).
[51] T. Thonhauser and C. Ambrosch-Draxl, Phys. Rev. B **67**, 134508 (2003).
[52] A. Dal Corso, A. Pasquarello, A. Baldereschi, and R. Car, Phys. Rev. B **53**, 1180 (1996).
[53] J. E. Jaffe, Z. Lin, and A. C. Hess, Phys. Rev. B **57**, 11834 (1998).
[54] C. Stampfl and C. G. Van de Walle, Phys. Rev. B **59**, 5521 (1999).
[55] F. Favot and A. Dal Corso, Phys. Rev. B **60**, 11427 (1999).
[56] C. Stampfl, W. Mannstadt, R. Asahi, and A. J. Freeman, Phys. Rev. B **63**, 155106 (2001).
[57] A. Janotti, S. H. Wei, and D. J. Singh, Phys. Rev. B **64**, 174107 (2001).
[58] N. Wakabayashi, Phys. Rev. B **33**, 6771 (1986).
[59] J. Zarestky, C. Stassis, B. N. Harmon, K. M. Ho, and C. L. Fu, Phys. Rev. B **28**, 697 (1983).
[60] O. De la Peña-Seaman, R. de Coss, R. Heid, and K. P. Bohnen, J. Phys.: Condens. Matter **19**, 476216 (2007).
[61] Spin-orbit coupling lifts the threefold degeneracy of this state. LAPW calculations including spin-orbit coupling indicate a small splitting of only 0.1 eV, which results in an uncertainty in x_c of ≈ 0.07.